SIMULATION OPTIMIZATION SYSTEMS
Research Laboratory

ELECTROMAGNETIC OPTIMIZATION EXPLOITING AGGRESSIVE SPACE MAPPING

J.W. Bandler, R.M. Biernacki, S.H. Chen,
R. H. Hemmers and K. Madsen

SOS-95-5-R

February 1995

McMASTER UNIVERSITY
Hamilton, Canada L8S 4L7
Department of Electrical and Computer Engineering

ELECTROMAGNETIC OPTIMIZATION EXPLOITING AGGRESSIVE SPACE MAPPING

J.W. Bandler, R.M. Biernacki, S.H. Chen,
R. H. Hemmers and K. Madsen

SOS-95-5-R

February 1995

© J.W. Bandler, R.M. Biernacki, S.H. Chen, R.H. Hemmers and K. Madsen 1995

No part of this document may be copied, translated, transcribed or entered in any form into any machine without written permission. Address enquiries in this regard to Dr. J.W. Bandler. Excerpts may be quoted for scholarly purposes with full acknowledgement of source. This document may not be lent or circulated without this title page and its original cover.

ELECTROMAGNETIC OPTIMIZATION EXPLOITING AGGRESSIVE SPACE MAPPING

John W. Bandler, *Fellow*, *IEEE*, Radoslaw M. Biernacki, *Senior Member*, *IEEE*, Shao Hua Chen, *Member*, *IEEE*, Ronald H. Hemmers, *Student Member*, *IEEE*, and Kaj Madsen

Abstract

We propose a significantly improved Space Mapping (SM) strategy for electromagnetic (EM) optimization. Instead of waiting for upfront EM analyses at several base points, our new approach aggressively exploits every available EM analysis, producing dramatic results right from the first step. We establish a relationship between the novel SM optimization and the quasi-Newton iteration for solving a system of nonlinear equations. Approximations to the matrix of first-order derivatives are updated by the classical Broyden formula. A high-temperature superconducting microstrip filter design solution emerges after fewer EM frequency sweeps than the number of designable parameters! Furthermore, less CPU effort is required to optimize the filter than is required by one single detailed frequency sweep. We also extend the SM concept to the parameter extraction phase, overcoming severely misaligned responses induced by inadequate empirical models. This novel concept should have a significant impact on parameter extraction of devices.

This work was supported in part by Optimization Systems Associates Inc., in part by the Natural Sciences and Engineering Research Council of Canada under Grants OGP0007239, OGP0042444 and STR0167080 and through the Micronet Network of Centres of Excellence. Additional support was provided through a Natural Sciences and Engineering Research Council of Canada Graduate Scholarship granted to R.H. Hemmers.

J.W. Bandler, R.M. Biernacki and S.H. Chen are with Optimization Systems Associates Inc., P.O. Box 8083, Dundas, Ontario, Canada L9H 5E7, and the Simulation Optimization Systems Research Laboratory and Department of Electrical and Computer Engineering, McMaster University, Hamilton, Ontario, Canada L8S 4L7.

R.H. Hemmers is with the Simulation Optimization Systems Research Laboratory and Department of Electrical and Computer Engineering, McMaster University, Hamilton, Ontario, Canada L8S 4L7.

K. Madsen is with the Institute of Mathematical Modeling, Technical University of Denmark, DK-2800 Lyngby, Denmark.

I. INTRODUCTION

In our recent pioneering work [1-3], we introduced the concept of Space Mapping (SM) optimization. The method combines the computational efficiency of empirical engineering circuit models, accumulated and developed over many years, with the acclaimed accuracy of electromagnetic (EM) simulators. This facilitates a highly efficient approach to attacking the demanding EM design process.

In our original formulation of the SM algorithm, an upfront effort was needed in the EM space simply to establish full-rank conditions leading to the initial mapping between the optimization and EM spaces. Since such initial base points are found by simple perturbation around the starting point in the EM space, they are unlikely to produce a substantially better design than the starting point itself. Hence, that approach represents a time-consuming and possibly unproductive effort.

In this paper, we present a significantly improved approach to SM. The method employs the quasi-Newton iteration in conjunction with first-order derivative approximations updated by the classical Broyden formula [4]. From an initial estimate of the EM solution, obtained by an empirical or coarse-grid EM model optimization, we target each costly EM analysis directly at achieving the best EM design. The results are then immediately utilized to improve the approximation. Using this approach, we expect to obtain a progressively improved design after each iteration. This procedure is based on an elegant theoretical formulation and a simple implementational strategy.

One of the key steps in SM is the model parameter identification phase. The SM technique relies on determining pairs of corresponding EM and empirical model points obtained by parameter extraction optimization. Accordingly, we review the appropriate theory and techniques used in traditional parameter extraction. In addition, we describe algorithms based on the idea of Frequency Space Mapping (FSM) [5]. They offer a powerful means of overcoming the problems caused by local minima and model misalignment.

Our new theory and techniques are illustrated through the design of a low-loss narrow-bandwidth high-temperature superconducting (HTS) microstrip filter [3, 5, 6]. We utilize the user-friendly OSA90/hope optimization system with the Empipe interface [7] to the Sonnet *em* field simulator [8].

In Section II, we review the original SM technique. In Section III, we introduce the theory and implementation of our new aggressive SM approach. Section IV reviews traditional parameter extraction optimization and our new FSM algorithms. Sections V-VIII illustrate the design of the HTS microstrip filter. Finally, Section IX contains our conclusions.

II. OVERVIEW OF THE ORIGINAL SPACE MAPPING METHOD

Let the behaviour of a system be described by models in two distinct spaces: the optimization space, denoted by X_{os}, and the EM (or validation) space, denoted by X_{em}. We represent the model parameters in these spaces by the vectors x_{os} and x_{em}, respectively. We assume that X_{os} and X_{em} have the same dimensionality, i.e., $x_{os} \in \mathbb{R}^n$ (X_{os}-space) and $x_{em} \in \mathbb{R}^n$ (X_{em}-space) but, in general, they may not represent the same parameters.

The X_{os}-space model can be comprised of empirical models [3, 5], or an efficient coarse-grid EM model [1, 2]. Typically, the X_{em}-space model is a fine-grid EM model [1-3, 5] but, ultimately, can represent actual hardware prototypes if time and resources permit. We assume that the X_{os}-space model responses, denoted by $R_{os}(x_{os})$, are much faster to calculate but less accurate than the X_{em}-space model responses, denoted by $R_{em}(x_{em})$.

In SM optimization, we wish to find a mapping, P, from the X_{em}-space to the X_{os}-space,

$$x_{os} = P(x_{em}) \tag{1}$$

such that

$$R_{os}(P(x_{em})) \approx R_{em}(x_{em}). \tag{2}$$

We assume that such a mapping exists and is one-to-one within some local modeling region encompassing our SM solution. We also assume that, based on (2), for a given x_{em} its image x_{os} in (1) can be found by a suitable parameter extraction procedure, and that this process is unique.

We initially perform optimization entirely in X_{os} to obtain the optimal design x_{os}^*, for instance in the minimax sense, and subsequently use SM to find the mapped solution $\bar{x}_{em}$ in X_{em} as

$$\bar{x}_{em} = P^{-1}(x_{os}^*) \tag{3}$$

once the mapping (1) is established (since we assume P is one-to-one, P^{-1} exists). This scenario is illustrated in Fig. 1. We designate $\bar{x}_{em}$ as the SM solution instead of x_{em}^* since the mapped solution may not be the true optimum in X_{em}, again for instance in the minimax sense.

The mapping is established through an iterative process. In our original work [1-3], we obtain the initial approximation of the mapping, $P^{(0)}$, by performing EM analyses at a preselected set of, at least, m base points in X_{em} around the starting point. Here, the first base point is

$$x_{em}^{(1)} = x_{os}^*, \tag{4}$$

followed by other points found by perturbation as

$$x_{em}^{(i)} = x_{em}^{(1)} + \Delta x_{em}^{(i-1)}, \quad i = 2, 3, ..., m \tag{5}$$

where m is the number of fundamental functions [1]. This is followed by parameter extraction optimization in X_{os} to obtain the set of corresponding base points $x_{os}^{(i)}$ for $i = 1, 2, ..., m$. The parameter extraction is carried out by the following optimization:

$$\underset{x_{os}^{(i)}}{\text{minimize}} \ \| R_{os}(x_{os}^{(i)}) - R_{em}(x_{em}^{(i)}) \| \tag{6}$$

for $i = 1, 2, ..., m$ where $\|\cdot\|$ indicates a suitable norm. The additional $m-1$ points apart from $x_{em}^{(1)}$ are required merely to establish full-rank conditions leading to our first approximation to the mapping. Hence, these EM analyses represent an upfront effort before any significant improvement over the starting point can be expected. With the high cost associated with each EM analysis, the additional $m-1$ simulations represent an inefficient component of the algorithm.

At the jth iteration, both sets may be expanded to contain, in general, m_j points which are used to establish the updated mapping $P^{(j)}$. Since the analytical form of P is not available, we use the current approximation $P^{(j)}$ to estimate $\bar{x}_{em}$ in (3), i.e.,

$$x_{em}^{(m_j+1)} = P^{(j)^{-1}}(x_{os}^*). \tag{7}$$

The process continues iteratively until the termination condition

$$\| R_{os}(x_{os}^{*}) - R_{em}(x_{em}^{(m_j+1)}) \| \leq \epsilon \tag{8}$$

is satisfied, where ϵ is a small positive constant. If so, $P^{(j)}$ is our desired P. If not, the set of base points in X_{em} is augmented by $x_{em}^{(m_j+1)}$ and correspondingly, $x_{os}^{(m_j+1)}$ determined by (6) augments the set of base points in X_{os}. Upon termination, we set $\bar{x}_{em} = x_{em}^{(m_j+1)} = P^{(j)^{-1}}(x_{os}^{*})$ as the SM solution. The original SM algorithm is illustrated graphically in Fig. 2.

III. AGGRESSIVE APPROACH TO SPACE MAPPING

Theory

Consider an important property of (8). When approaching the SM solution, the optimal X_{os}-space model response $R_{os}(x_{os}^{*})$ will closely match the X_{em}-space model response $R_{em}(x_{em}^{(m_j+1)})$, within some tolerance ϵ. Hence, after performing an additional parameter extraction optimization in X_{os}, the resulting point $x_{os}^{(m_j+1)} = P(x_{em}^{(m_j+1)})$ should approach x_{os}^{*}. Stated more precisely, as $j \rightarrow M$, $x_{os}^{(m_j+1)} \rightarrow x_{os}^{*}$, or

$$\| x_{os}^{(m_j+1)} - x_{os}^{*} \| \leq \eta \quad \text{as} \quad j \rightarrow M \tag{9}$$

where η is a small positive constant and M is the number of iterations needed to converge to an SM solution.

Based on this observation, we can now introduce our new approach. As in (1), we assume that the vector of X_{os}-space model parameters is a nonlinear vector function, P, of the X_{em}-space model parameters (due to any inherent nonlinearity between the two models). We define our goal by setting η to 0 in (9). Hence, we consider the set of n nonlinear equations

$$f(x_{em}) = 0 \tag{10}$$

of the form

$$f(x_{em}) = P(x_{em}) - x_{os}^{*} \tag{11}$$

where x_{os}^{*} is a given vector (optimal solution in X_{os}).

Let $x_{em}^{(j)}$ be the jth approximation to the solution of (10) and $f^{(j)}$ written for $f(x_{em}^{(j)})$. Based on $f^{(1)}, f^{(2)}, ..., f^{(j)}$ (found by parameter extraction (6) in all previous iterations), an approximation $B^{(j)}$ to the Jacobian matrix $J(x_{em}^{(j)})$,

$$J(x_{em}^{(j)}) = \left[\frac{\partial f^T(x_{em}^{(j)})}{\partial x_{em}}\right]^T, \tag{12}$$

is established. Since the Jacobian matrix is not available, the next iterate $x_{em}^{(j+1)}$ is found by a quasi-Newton iteration with $J(x_{em}^{(j)})$ replaced by $B^{(j)}$ as

$$x_{em}^{(j+1)} = x_{em}^{(j)} + h^{(j)} \tag{13}$$

where $h^{(j)}$ solves the linear system

$$B^{(j)}h^{(j)} = -f^{(j)}. \tag{14}$$

Thus, combining (13) and (14), the quasi-Newton iteration is

$$x_{em}^{(j+1)} = x_{em}^{(j)} - B^{(j)^{-1}}f^{(j)} \tag{15}$$

assuming $B^{(j)}$ is non-singular. The next approximation $B^{(j+1)}$ to the Jacobian matrix is found by the classical Broyden updating formula [4] as

$$B^{(j+1)} = B^{(j)} + \frac{f(x_{em}^{(j)} + h^{(j)}) - f(x_{em}^{(j)}) - B^{(j)}h^{(j)}}{h^{(j)^T}h^{(j)}}\, h^{(j)^T}. \tag{16}$$

Incorporating (14) into (16) gives a simplified updating formula

$$B^{(j+1)} = B^{(j)} + \frac{f^{(j+1)}h^{(j)^T}}{h^{(j)^T}h^{(j)}} \tag{17}$$

where $f^{(j+1)}$ is (11) evaluated at $x_{em}^{(j+1)}$ using the parameter extraction optimization as in (6). In our current implementation, the initial approximation $B^{(1)}$ to the Jacobian matrix is set to the identity matrix.

This new approach is significantly more efficient than our original SM algorithm. The reason for this is that we target every valuable EM analysis for the purpose of improving our estimate of the solution. In other words, $x_{em}^{(j+1)}$ is generated not merely as a base point for establishing the mapping, but to solve the nonlinear system of equations (10). Using the new

method, we avert from performing time-consuming and possibly unproductive EM analyses at perturbations around the starting point (4). Instead, we begin with a straightforward initial estimate and attempt to improve the EM design in a systematic manner free of *ad hoc* decisions. Our quasi-Newton approach to SM is illustrated graphically in Fig. 3.

Implementation

We now present a straightforward implementation of our new aggressive SM algorithm. We begin with a point, $\boldsymbol{x}_{os}^{*} \triangleq arg\min\{F(\boldsymbol{x}_{os})\}$, representing the optimal design in the $\boldsymbol{X}_{os}$-space where $F(\boldsymbol{x}_{os})$ is some appropriate objective function. Then, our algorithm proceeds as follows:

Step 0. Initialize $\boldsymbol{x}_{em}^{(1)} = \boldsymbol{x}_{os}^{*}$, $\boldsymbol{B}^{(1)} = \boldsymbol{1}$, $\boldsymbol{f}^{(1)} = \boldsymbol{P}(\boldsymbol{x}_{em}^{(1)}) - \boldsymbol{x}_{os}^{*}$, $j = 1$. Stop if $\| \boldsymbol{f}^{(1)} \| \leq \eta$.

Step 1. Solve $\boldsymbol{B}^{(j)}\boldsymbol{h}^{(j)} = -\boldsymbol{f}^{(j)}$ for $\boldsymbol{h}^{(j)}$.

Step 2. Set $\boldsymbol{x}_{em}^{(j+1)} = \boldsymbol{x}_{em}^{(j)} + \boldsymbol{h}^{(j)}$.

Step 3. Evaluate $\boldsymbol{P}(\boldsymbol{x}_{em}^{(j+1)})$ by parameter extraction.

Step 4. Compute $\boldsymbol{f}^{(j+1)} = \boldsymbol{P}(\boldsymbol{x}_{em}^{(j+1)}) - \boldsymbol{x}_{os}^{*}$. If $\| \boldsymbol{f}^{(j+1)} \| \leq \eta$, stop.

Step 5. Update $\boldsymbol{B}^{(j)}$ to $\boldsymbol{B}^{(j+1)}$.

Step 6. Set $j = j + 1$; go to *Step* 1.

IV. MODEL PARAMETER IDENTIFICATION

Review of Traditional Parameter Extraction

One of the key steps of SM involves parameter extraction optimization in order to match responses. For each $\boldsymbol{X}_{em}$-space point $\boldsymbol{x}_{em}$ we need to find a corresponding $\boldsymbol{X}_{os}$-space point $\boldsymbol{x}_{os}$. Assuming our response of interest is a function of frequency, let

$$\boldsymbol{R}_{em}(\boldsymbol{x}_{em}, \omega) \triangleq [\, R_{em_1}(\boldsymbol{x}_{em}) \;\; R_{em_2}(\boldsymbol{x}_{em}) \;\; \ldots \;\; R_{em_k}(\boldsymbol{x}_{em}) \,]^{T} \tag{18}$$

represent the $\boldsymbol{X}_{em}$-space model response simulated at k frequency points ω_i for $i = 1, 2, \ldots, k$ where

$$R_{em_i}(\boldsymbol{x}_{em}) \triangleq R_{em}(\boldsymbol{x}_{em}, \omega_i), \quad i = 1, 2, \ldots, k. \tag{19}$$

Also, let

$$\boldsymbol{R}_{os}(\boldsymbol{x}_{os}, \omega) \triangleq [\, R_{os_1}(\boldsymbol{x}_{os}) \;\; R_{os_2}(\boldsymbol{x}_{os}) \;\; \ldots \;\; R_{os_k}(\boldsymbol{x}_{os}) \,]^T \tag{20}$$

represent the $\boldsymbol{X}_{os}$-space model response where

$$R_{os_i}(\boldsymbol{x}_{os}) \triangleq R_{os}(\boldsymbol{x}_{os}, \omega_i), \quad i = 1, 2, \ldots, k. \tag{21}$$

Thus, the identification problem can be formulated by minimizing a scalar objective function, H, based on a set of k error functions given as

$$\boldsymbol{e}(\boldsymbol{x}_{os}, \omega) \triangleq [\, e_1(\boldsymbol{x}_{os}) \;\; e_2(\boldsymbol{x}_{os}) \;\; \ldots \;\; e_k(\boldsymbol{x}_{os}) \,]^T \tag{22}$$

of the form

$$e_i(\boldsymbol{x}_{os}) \triangleq e(\boldsymbol{x}_{os}, \omega_i) = w_i[R_{os_i}(\boldsymbol{x}_{os}) - R_{em_i}(\boldsymbol{x}_{em})], \quad i = 1, 2, \ldots, k \tag{23}$$

where w_i are some nonnegative weighting factors. Note, in our parameter extraction formulation $\boldsymbol{x}_{em}$ and hence $\boldsymbol{R}_{em}(\boldsymbol{x}_{em}, \omega)$ are fixed while the elements in $\boldsymbol{x}_{os}$ are optimized.

Thus, the parameter extraction problem is described by

$$\underset{\boldsymbol{x}_{os}}{\text{minimize}} \;\; H(\boldsymbol{x}_{os}) \tag{24}$$

where H is typically formulated as an ℓ_p-norm of the error functions [9]. One choice for H could be the popular ℓ_2, or least-squares objective

$$H = \sum_{i=1}^{k} \left[e_i(\boldsymbol{x}_{os}) \right]^2 \tag{25}$$

but, we may wish to use the ℓ_1-norm given by

$$H = \sum_{i=1}^{k} \left| e_i(\boldsymbol{x}_{os}) \right| \tag{26}$$

which is robust against gross errors. Alternatively, we may consider the novel Huber-norm [10, 11]

$$H = \sum_{i=1}^{k} \rho_k(e_i(\boldsymbol{x}_{os})) \tag{27}$$

where

$$\rho_k(e_i) \triangleq \begin{cases} e_i^2/2 & \text{if } |e_i| \le k \\ k|e_i| - k^2/2 & \text{if } |e_i| > k \end{cases} \tag{28}$$

which is robust against large errors *and* flexible w.r.t. small variations in the data.

As noted earlier, parameter extraction is an important step in SM. This can be a serious challenge, especially at the starting point if the X_{os}-space model and X_{em}-space model responses are severely misaligned. If we perform straightforward data-fitting optimization from such a starting point using the traditional approach, the process can easily be trapped by local minima [5]. To address this issue, we explore significant enhancements to traditional parameter extraction.

A New Approach: Frequency Space Mapping (FSM)

At a given point, typically we will observe a general similarity between the responses R_{os} and R_{em} even if they are severely misaligned. With this in mind, the parameter extraction problem can be better conditioned if we align R_{os} and R_{em} along the frequency axis first. Specifically, R_{em} is kept fixed while we adjust R_{os} in some appropriate manner. This is accomplished by employing a reference angular frequency $\omega = \omega_{em}$ and a transformed angular frequency ω_{os} related by

$$\omega_{os} = P_{\omega}(\omega). \tag{29}$$

For our purposes, a suitable mapping can be as simple as frequency shift and scaling given by

$$\omega_{os} = \sigma\omega + \delta \tag{30}$$

where σ represents a scaling factor and δ an offset.

This brings us to *Phase* 1 of our FSM approach. We need to determine σ_o and δ_o, which would effectively align R_{os} and R_{em} in the frequency domain. This is done by holding both model parameters x_{os} and x_{em} constant and optimizing only the parameters σ_o and δ_o. This is described by the following optimization:

$$\underset{\sigma_o,\,\delta_o}{\text{minimize}} \; \| R_{os}(x_{os}, \sigma_o\omega + \delta_o) - R_{em}(x_{em}, \omega) \| \tag{31}$$

where $\|\cdot\|$ is typically the ℓ_2, ℓ_1 or Huber norm.

In *Phase* 2 of our FSM approach, we optimize the X_{os}-space model parameters x_{os} such that R_{os} matches R_{em} while x_{em} again remains fixed. In addition, we optimize σ and δ to obtain the identity mapping starting from $\sigma = \sigma_o$ and $\delta = \delta_o$. We have developed three algorithms to realize this

goal: a sequential FSM algorithm (SFSM) and two exact-penalty function algorithms (EPF), one based on the ℓ_1-norm objective while the other is suitable for minimax optimization.

In the SFSM algorithm, we perform a sequence of optimizations in which the frequency mapping is *gradually* reduced to the identity mapping while $\boldsymbol{x}_{os}$ is optimized at each step. Hence, at the jth iteration of the SFSM algorithm we set both $\sigma^{(j)}$ and $\delta^{(j)}$ and then optimize $\boldsymbol{x}_{os}^{(j)}$ such that $\boldsymbol{R}_{os}$ best matches $\boldsymbol{R}_{em}$. This can be written as

$$\underset{\boldsymbol{x}_{os}^{(j)}}{\text{minimize}} \; \| \boldsymbol{R}_{os}(\boldsymbol{x}_{os}^{(j)}, \sigma^{(j)}\omega + \delta^{(j)}) - \boldsymbol{R}_{em}(\boldsymbol{x}_{em}, \omega) \|, \quad j = 0, 1, \ldots, K \tag{32}$$

where

$$\sigma^{(j)} = 1 + (\sigma_o - 1)\frac{(K - j)}{K} \tag{33}$$

and

$$\delta^{(j)} = \delta_o \frac{(K - j)}{K} \tag{34}$$

where K determines the number of steps in the sequence. After the sequence of optimizations, $\boldsymbol{x}_{os}^{(K)}$ is the solution to the parameter extraction problem since $\sigma^{(K)} = 1$ and $\delta^{(K)} = 0$. It should be clear that for larger values of K we increase the probability of success in the parameter extraction problem at the expense of longer optimization time.

In the EPF algorithms, we need to perform only one optimization. The ℓ_1-norm version of the EPF formulation is given by

$$\underset{\boldsymbol{x}_{os}, \sigma, \delta}{\text{minimize}} \; \{ \| \boldsymbol{R}_{os}(\boldsymbol{x}_{os}, \sigma\omega + \delta) - \boldsymbol{R}_{em}(\boldsymbol{x}_{em}, \omega) \|_1 + \alpha_1 |\sigma - 1| + \alpha_2 |\delta| \} \tag{35}$$

where α_1 and α_2 are suitably large positive weighting factors. In the minimax version of the EPF formulation [12], we have

$$\underset{\boldsymbol{x}_{os}, \boldsymbol{\alpha}, \sigma, \delta}{\text{minimize}} \left\{ \max_{1 \le i \le 4} \left(U(\boldsymbol{x}_{os}, \sigma, \delta), \; U(\boldsymbol{x}_{os}, \sigma, \delta) - \alpha_i c_i \right) \right\} \tag{36}$$

where

$$U(\boldsymbol{x}_{os}, \sigma, \delta) = \| \boldsymbol{R}_{os}(\boldsymbol{x}_{os}, \sigma\omega + \delta) - \boldsymbol{R}_{em}(\boldsymbol{x}_{em}, \omega) \|, \tag{37}$$

$$\boldsymbol{c}(\sigma, \delta) = \begin{bmatrix} \sigma - 1 \\ -(\sigma - 1) \\ \delta \\ -(\delta) \end{bmatrix} \tag{38}$$

and $\alpha_i > 0$ for $i = 1, 2, 3, 4$. For both EPF formulations, the values of α_i are kept fixed and must be sufficiently large to obtain the identity mapping in (30) and hence the solution to the parameter extraction optimization.

While the frequency transformation concept is familiar to microwave engineers, particularly filter designers, here it is defined in a novel way. Our FSM is established through an iterative process and facilitates automated compensation for inadequate modeling. This significantly improves robustness of the parameter extraction phase of the overall SM technique as needed in (6).

V. THE HTS FILTER

We consider the design of a four-pole quarter-wave parallel coupled-line microstrip filter, as illustrated in Fig. 4 [3, 5]. L_1, L_2 and L_3 are the lengths of the parallel coupled-line sections and S_1, S_2 and S_3 are the gaps between the sections. The width $W = 7$ mil is the same for all the sections as well as for the input and output microstrip lines. The input and output line lengths are $L_0 = 50$ mil. The thickness of the lanthanum aluminate substrate used is 20 mil and the dielectric constant is assumed to be 23.425. The design specifications imposed on $|S_{21}|$ are as follows:

$$|S_{21}| \leq 0.05 \quad \text{in the stopband} \quad (f \leq 3.967 \text{ GHz and } f \geq 4.099 \text{ GHz})$$
$$|S_{21}| \geq 0.95 \quad \text{in the passband} \quad (4.008 \text{ GHz} \leq f \leq 4.058 \text{ GHz})$$

where f is frequency. This corresponds to a 1.25% bandwidth. L_1, L_2, L_3, S_1, S_2 and S_3 are considered as design parameters. L_0 and W are kept fixed.

We employ both analytical/empirical models available in OSA90/hope and a fine-grid Sonnet *em* model. The HTS filter empirical model is assembled from fundamental components such as microstrip lines, coupled lines and open stubs. The OSA90/hope empirical model and Sonnet *em* model material and physical parameters are listed in Table I. They are fixed. On a Sun

SPARCstation 10, approximately 1 CPU hour is needed to simulate the filter at a single frequency for an on-grid point.

VI. EMPIRICAL MODEL DESIGN OF THE HTS FILTER

For the empirical model frequency-domain design of the HTS filter, we consider the minimization of a scalar objective function, say G, which provides a measure of the deviation of the $|S_{21}|$ filter response from the imposed design specifications. In order to formulate G we consider error functions, $g_i(\boldsymbol{x}_{os})$, defined as

$$g_i(\boldsymbol{x}_{os}) = R_{os}(\boldsymbol{x}_{os}, \omega_i) - S_u(\omega_i) \quad \text{or} \quad g_i(\boldsymbol{x}_{os}) = S_l(\omega_i) - R_{os}(\boldsymbol{x}_{os}, \omega_i) \tag{39}$$

where $S_u(\omega_i)$ and $S_l(\omega_i)$ are the upper and lower specifications, respectively, and $R_{os}(\boldsymbol{x}_{os}, \omega_i)$ is the empirical model response of the filter at a given point of the designable parameters $\boldsymbol{x}_{os}$. The errors are computed at frequencies for which S_u and/or S_l are specified. A negative error value indicates that the corresponding specification is satisfied. For positive error values the corresponding specifications are violated. For filter design, we make use of the generalized minimax objective function

$$G = \max_i \{g_i(\boldsymbol{x}_{os})\}. \tag{40}$$

We started the design of the HTS filter using an OSA90/hope empirical model. The minimax solution is listed in Table II(a). Fig. 5 shows the $|S_{21}|$ and $|S_{11}|$ responses after optimization.

Next, we investigate the robustness of the empirical model nominal solution. The same optimization variables, namely L_1, L_2, L_3, S_1, S_2 and S_3 as in the nominal minimax design are selected. Again, L_0 and W are kept fixed. We perform a number of empirical model minimax optimizations, each starting from a different starting point. We use 50 starting points randomly spread around the minimax solution with a ±1% deviation. Fig. 6(a) plots the $|S_{21}|$ responses for all 50 starting points. The bar chart in Fig. 6(b) depicts the Euclidian distances between the reference minimax solution and the perturbed starting points. Fig. 7 shows the corresponding diagrams after minimax optimizations. Figs. 7(b) and 7(c) clearly illustrate the existence of multiple

minimax solutions for the HTS filter. Table II(b) lists a second minimax solution. Fig. 8 compares the $|S_{21}|$ and $|S_{11}|$ responses between the two solutions. The responses exhibit similarity despite the large numerical deviation in the parameter values.

We perform EM analyses at the two minimax solutions. The ***em*** results differ significantly from the empirical model responses, as shown in Fig. 9. However, the two ***em*** analyses exhibit strong similarity. Our aim then, is to use SM to find a solution in the EM space which will substantially reproduce the optimal performance predicted by the empirical model.

VII. ILLUSTRATION OF FSM

A critical step in SM is parameter extraction optimization to match the empirical model response to the EM model response. At the starting point, the empirical and EM model responses may be severely misaligned, as shown in Fig. 10. If we perform a straightforward ℓ_1 optimization from such a starting point, the extraction process can be trapped by a local minimum, as illustrated in Figs. 11 and 12.

We apply our new FSM approach to overcome the difficulties imposed by local minima. First, *Phase* 1 aligns $\boldsymbol{R}_{os}$ and $\boldsymbol{R}_{em}$ along the frequency axis by optimizing the frequency shift and scaling parameters while holding $\boldsymbol{x}_{os}$ and $\boldsymbol{x}_{em}$ fixed, with $\boldsymbol{x}_{os} = \boldsymbol{x}_{em}$. The result is shown in Fig. 13. Next, we initiate *Phase* 2 employing the SFSM algorithm setting $K = 5$ to obtain both the identity mapping and the optimal values of $\boldsymbol{x}_{os}$. Fig. 14 depicts the resulting response match using the SFSM algorithm. Fig. 15 compares the $|S_{21}|$ match between the straightforward ℓ_1 optimization and the SFSM algorithm.

VIII. AGGRESSIVE SM OPTIMIZATION OF THE HTS FILTER

We perform SM optimization applying our new quasi-Newton SM algorithm with the Broyden update starting from the empirical model minimax solution (a) listed in Table II. The SM solution is listed in Table III. We require only 7 frequency points per EM frequency sweep. The

solution emerges after only 4 EM analyses (frequency sweeps). Fig. 16 compares the filter responses of the empirical model optimal design and the ***em*** simulated SM solution.

IX. CONCLUSIONS

We have proposed a new automated SM approach which aggressively exploits every EM analysis. We have employed the classical Broyden update to target the next EM point at the optimal design. We have described and demonstrated our new approach to the EM design of an HTS microstrip filter. We have pioneered the application of the SM concept to parameter extraction by developing new FSM algorithms for overcoming poor starting points induced by inadequate empirical models.

ACKNOWLEDGEMENT

The authors thank Dr. J.C. Rautio, President of Sonnet Software, Inc., Liverpool, NY, for making ***em*** available for this work.

REFERENCES

[1] J.W. Bandler, R.M. Biernacki, S.H. Chen, P.A. Grobelny and R.H. Hemmers, "Space mapping technique for electromagnetic optimization," *IEEE Trans. Microwave Theory Tech.*, vol. 42, 1994, pp. 2536-2544.

[2] J.W. Bandler, R.M. Biernacki, S.H. Chen, P.A. Grobelny and R.H. Hemmers, "Exploitation of coarse grid for electromagnetic optimization," *IEEE MTT-S Int. Microwave Symp. Dig.* (San Diego, CA), 1994, pp. 381-384.

[3] J.W. Bandler, R.M. Biernacki, S.H. Chen, P.A. Grobelny, C. Moskowitz and S.H. Talisa, "Electromagnetic design of high-temperature superconducting microwave filters," *IEEE MTT-S Int. Microwave Symp. Dig.* (San Diego, CA), 1994, pp. 993-996.

[4] C.G. Broyden, "A class of methods for solving nonlinear simultaneous equations," *Math. of Comp.*, vol. 19, 1965, pp. 577-593.

[5] J.W. Bandler, R.M. Biernacki, S.H. Chen, R.H. Hemmers and K. Madsen, "Aggressive space mapping for electromagnetic design," *IEEE MTT-S Int. Microwave Symp. Dig.* (Orlando, FL), 1995.

[6] S.H. Talisa, M.A. Janocko, C. Moskowitz, J. Talvacchio, J.F. Billing, R. Brown, D.C. Buck, C.K. Jones, B.R. McAvoy, G.R. Wagner and D.H. Watt, "Low- and high-temperature

superconducting microwave filters," *IEEE Trans. Microwave Theory Tech.*, vol. 39, 1991, pp. 1448-1454.

[7] *OSA90/hope*™ and *Empipe*™, Optimization Systems Associates Inc., P.O. Box 8083, Dundas, Ontario, Canada L9H 5E7, 1994.

[8] ***em***™ and ***xgeom***™, Sonnet Software, Inc., 135 Old Cove Road, Suite 203, Liverpool, NY 13090-3774, 1994.

[9] J.W. Bandler and S.H. Chen, "Circuit optimization: the state of the art," *IEEE Trans. Microwave Theory Tech.*, vol. 36, 1988, pp. 424-443.

[10] J.W. Bandler, S.H. Chen, R.M. Biernacki, L. Gao, K. Madsen and H. Yu, "Huber optimization of circuits: a robust approach," *IEEE Trans. Microwave Theory Tech.*, vol. 41, 1993, pp. 2279-2287.

[11] J.W. Bandler, S.H. Chen, R.M. Biernacki and K. Madsen, "The Huber concept in device modeling, circuit diagnosis and design centering," *Proc. IEEE Int. Symp. Circuits and Systems* (London, England), 1994, vol. 1, pp. 129-132.

[12] J.W. Bandler and C. Charalambous, "Nonlinear programming using minimax techniques," *J. Optim. Theory and Appl.*, vol. 13, 1974, pp. 607-619.

TABLE I

MATERIAL AND PHYSICAL PARAMETERS FOR THE OSA90/hope AND *em* MODELS

Model Parameters	OSA90/hope Model Parameter Values	*em* Model Parameter Values
EPSR	23.425	23.425
H (mil)	19.9516	19.9516
H2 (mil)	∞	250
T (mil)	1.9685E-2	0
TAND	3.0E-5	3.0E-5
ROC* (Ωm)	0	4.032E-8
RHS (mil)	0	-
MTAND	-	0
SR (Ω/sq)	-	0
XCELL (mil)	-	1
YCELL (mil)	-	1.75

EPSR: dielectric constant of the substrate
H: substrate thickness
H2: shielding cover height
T: conducting metal thickness
TAND: substrate dielectric loss tangent
ROC: resistivity of the conducting strip
RHS: surface roughness of the metal strip
MTAND: magnetic loss tangent
SR: surface reactance
XCELL: x-grid cell size
YCELL: y-grid cell size

* in *em* ROC is represented by RHO

TABLE II

HTS FILTER EMPIRICAL MODEL DESIGN RESULTS

Parameter (mil)	Minimax Solution (a)	Minimax Solution (b)
L_1	188.33	137.4
L_2	197.98	248
L_3	188.58	138.6
S_1	21.97	17.35
S_2	99.12	120.9
S_3	111.67	75.9

W and L_0 are kept fixed at 7 mil and 50 mil, respectively.

TABLE III

SM OPTIMIZATION RESULTS

Parameter (mil)	SM Solution
L_1	186
L_2	196
L_3	185
S_1	21
S_2	80.5
S_3	85.75
Number of EM Analyses	4

All parameter values are rounded to the nearest grid-point. W and L_0 are kept fixed at 7 mil and 50 mil, respectively.

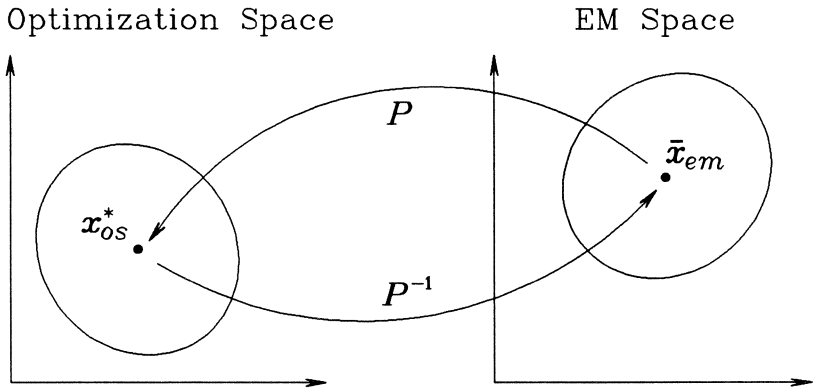

Fig. 1. Illustration of SM. The inverse mapping P^{-1} maps the optimal design x^*_{os} to $\bar{x}_{em}$ in the EM space.

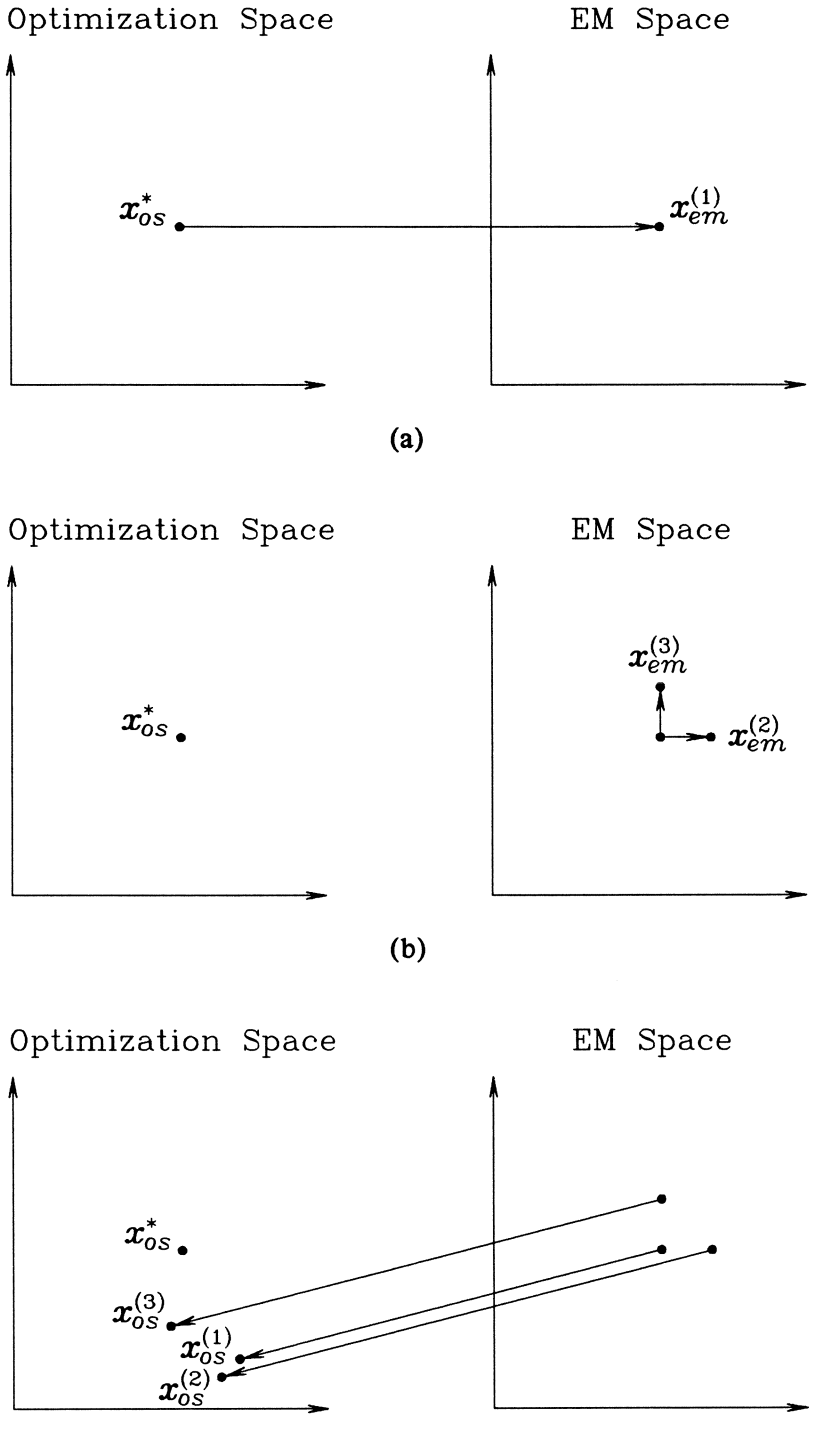

Fig. 2. Illustration of the original SM algorithm: (a) set $x_{em}^{(1)} = x_{os}^*$, (b) generate, at least, $m-1$ additional base points around $x_{em}^{(1)}$, (c) perform X_{os}-space model parameter extraction according to (6).

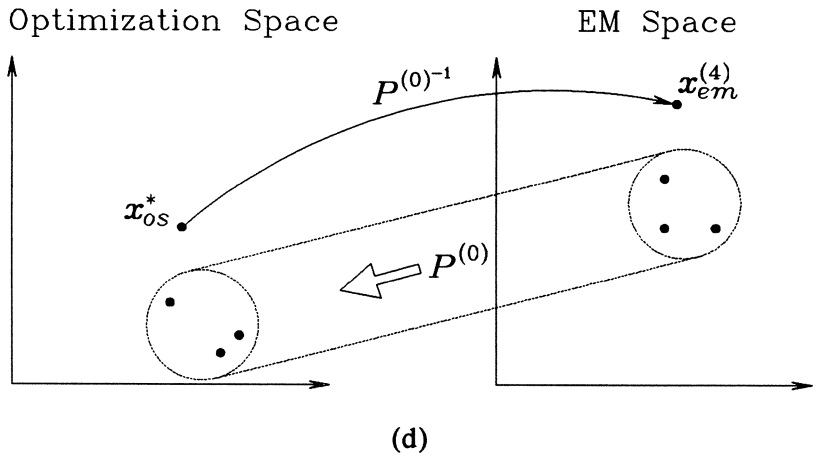

(d)

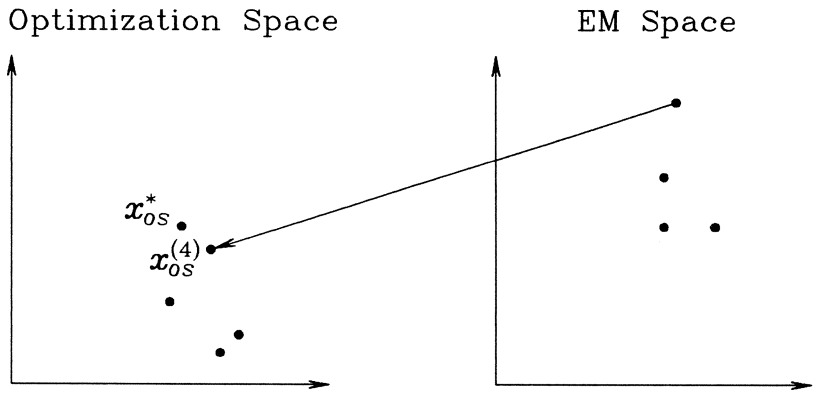

(e)

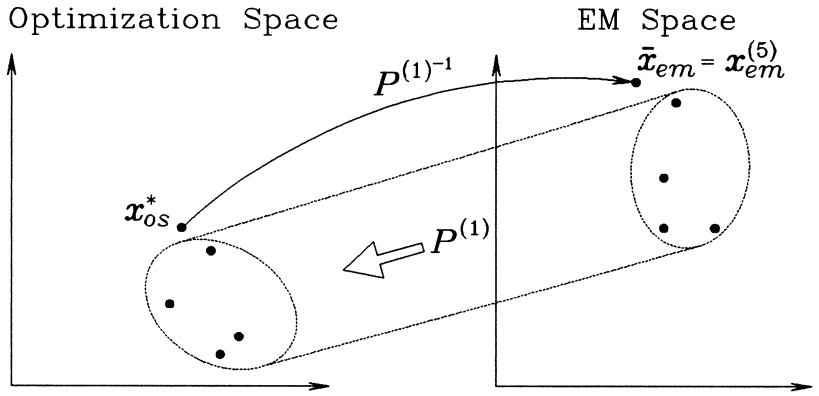

(f)

Fig. 2. Illustration of the original SM algorithm (cont.): (d) apply the inverse mapping to obtain the next X_{em}-space point $x_{em}^{(4)}$, (e) perform X_{os}-space model parameter extraction to obtain $x_{os}^{(4)}$, (f) apply the updated inverse mapping to obtain the SM solution $\bar{x}_{em} = x_{em}^{(5)}$, assuming $\| R_{os}(x_{os}^{*}) - R_{em}(x_{em}^{(5)}) \| \leq \epsilon$.

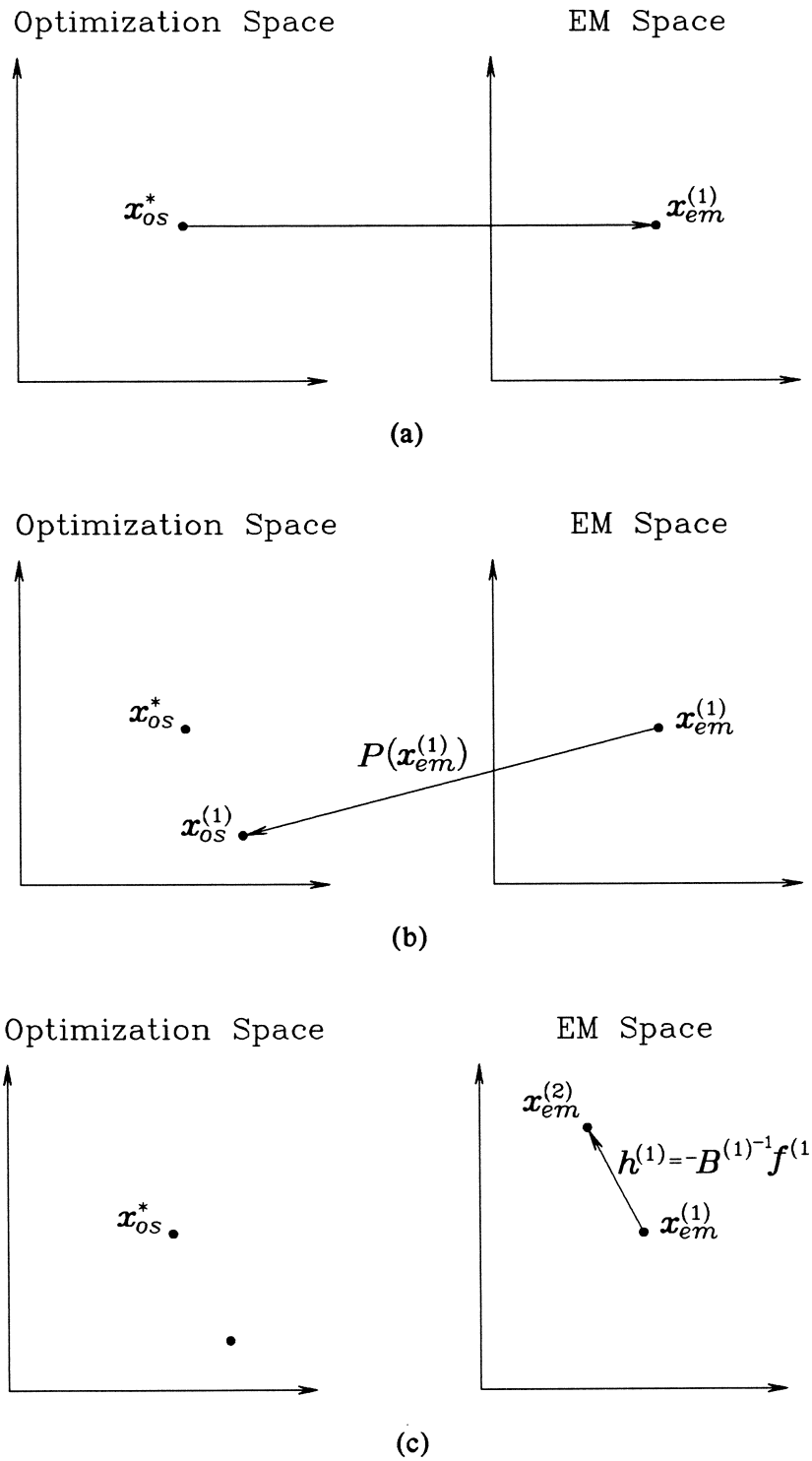

Fig. 3. Illustration of the quasi-Newton SM algorithm: (a) Initialize $x_{em}^{(1)} = x_{os}^*$ and $B^{(1)} = 1$, (b) perform X_{os}-space model parameter extraction according to (6), (c) obtain $x_{em}^{(2)}$ by solving $B^{(1)}h^{(1)} = -f^{(1)}$ for $h^{(1)}$.

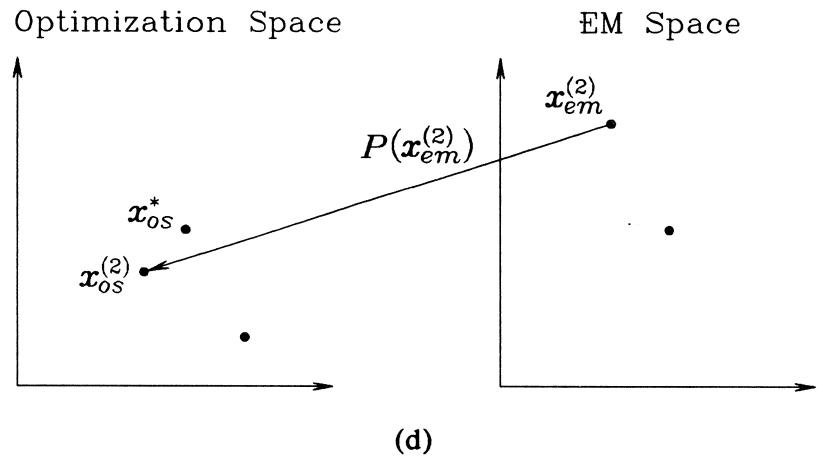

(d)

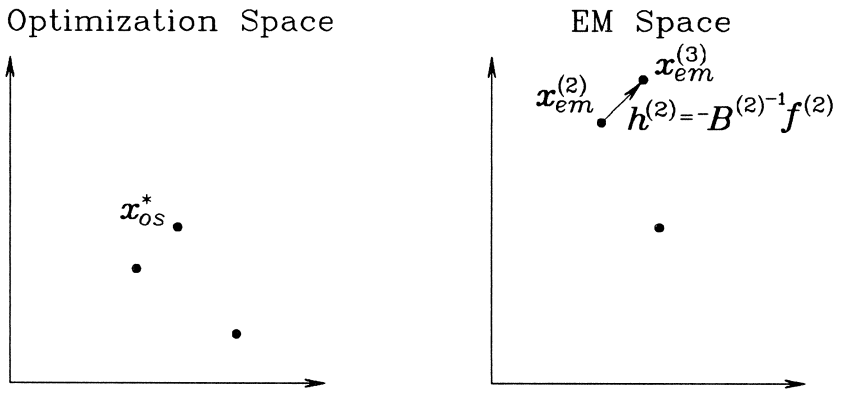

(e)

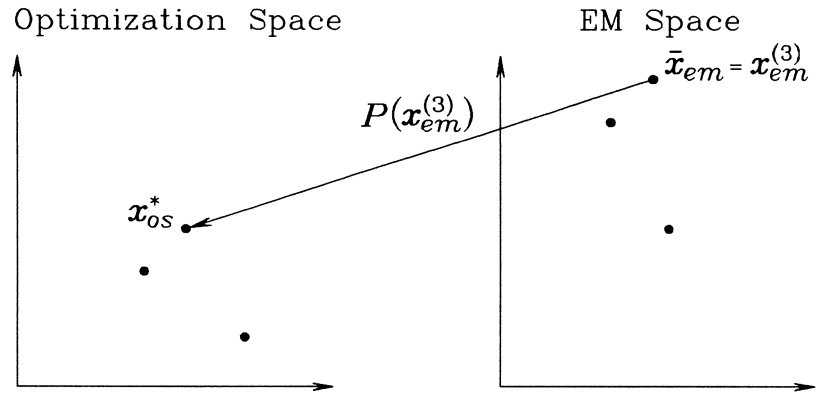

(f)

Fig. 3. Illustration of the quasi-Newton SM algorithm (cont.): (d) perform X_{os}-space model parameter extraction to obtain $x_{os}^{(2)}$, (e) obtain $x_{em}^{(3)}$ by solving $B^{(2)}h^{(2)} = -f^{(2)}$ for $h^{(2)}$, (f) the SM solution is $\bar{x}_{em} = x_{em}^{(3)}$ assuming $\| x_{os}^{(3)} - x_{os}^{*} \| \leq \eta$.

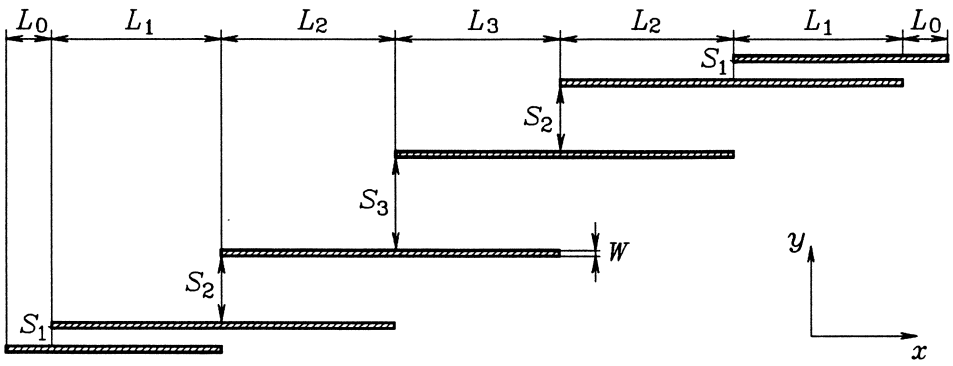

Fig. 4. The structure of the HTS filter [3, 5].

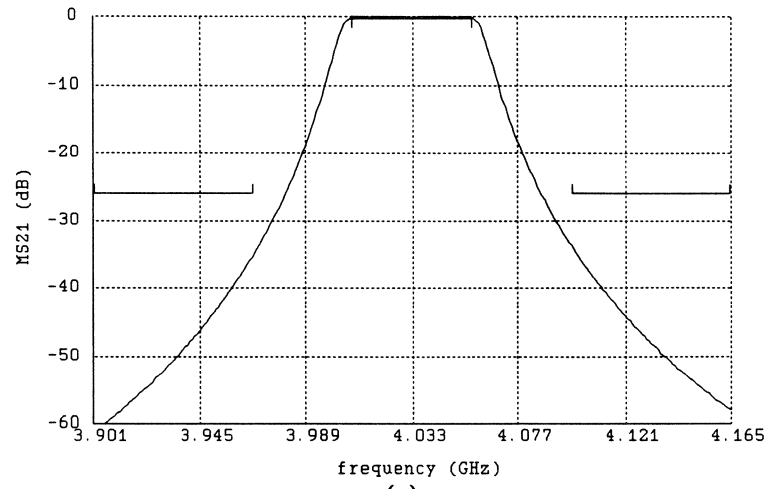

(a)

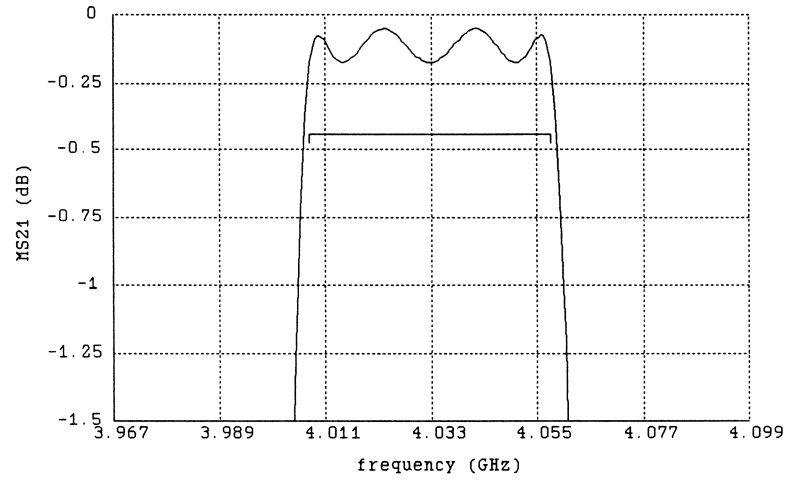

(b)

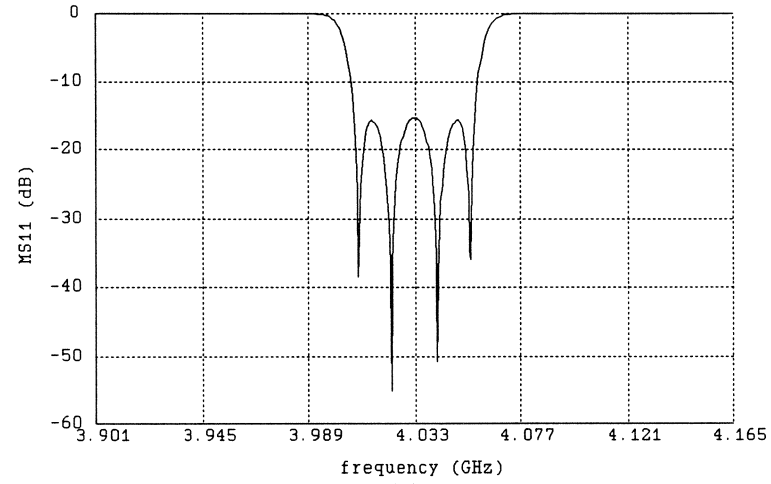

(c)

Fig. 5. The OSA90/hope empirical model responses after minimax optimization. The $|S_{21}|$ response for (a) the overall band and (b) the passband details. (c) The $|S_{11}|$ response of the filter.

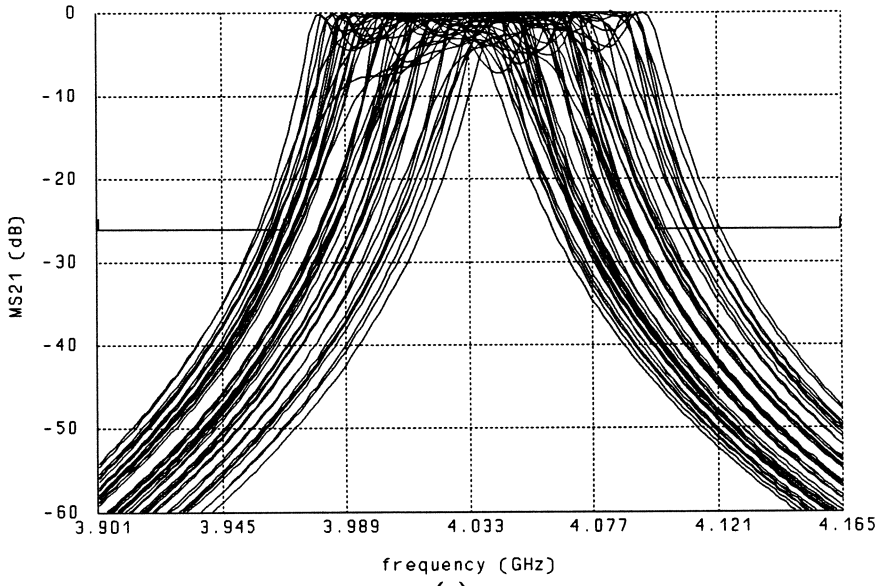

(a)

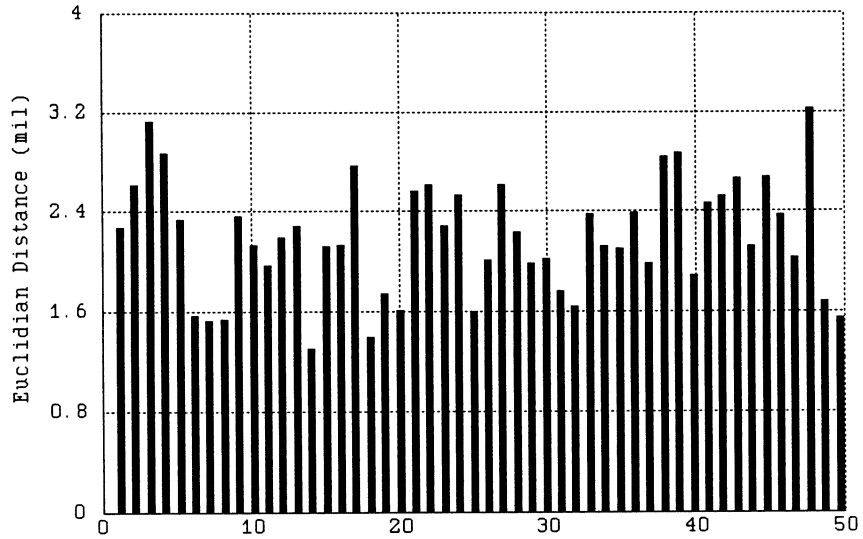

(b)

Fig. 6. (a) The empirical model $|S_{21}|$ responses at 50 random starting points and (b) the Euclidian distances between the perturbed starting points and the reference minimax solution.

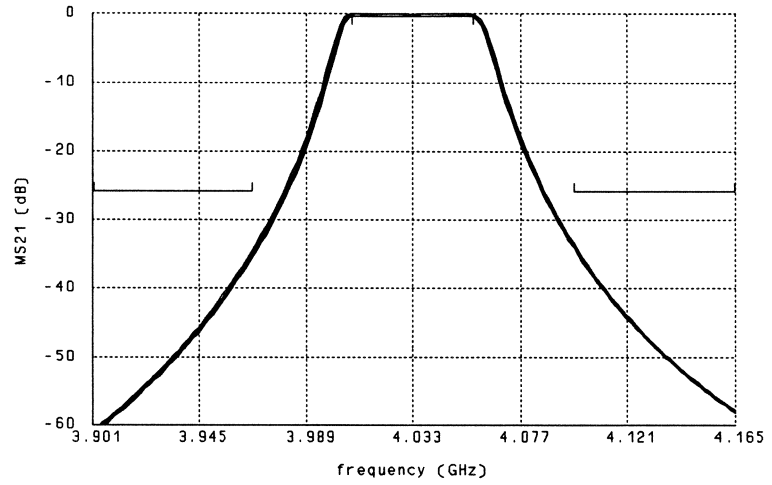

(a)

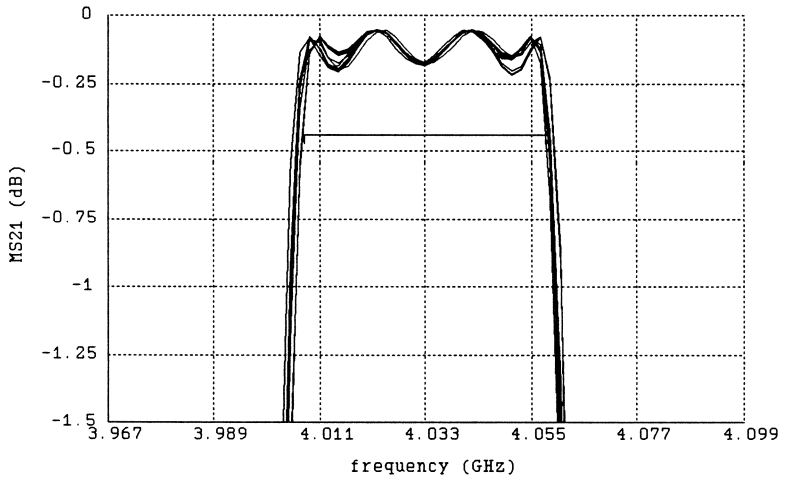

(b)

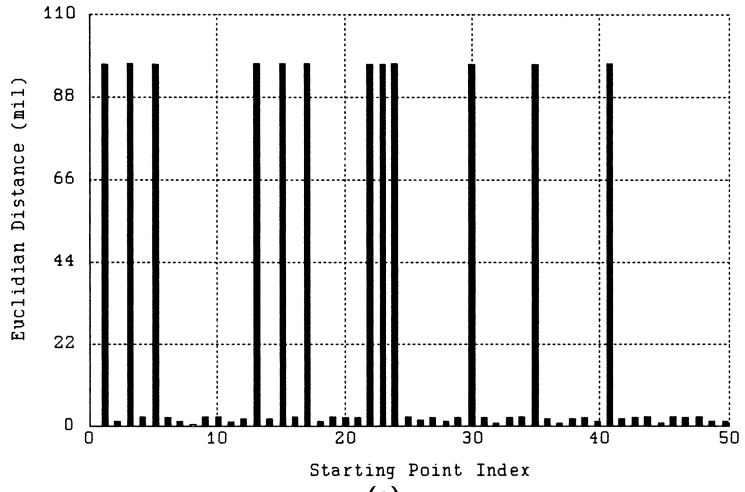

(c)

Fig. 7. The empirical model $|S_{21}|$ responses at the 50 optimized solutions for (a) the overall band, (b) the passband in more detail and (c) the Euclidian distances between the optimized and reference minimax solution.

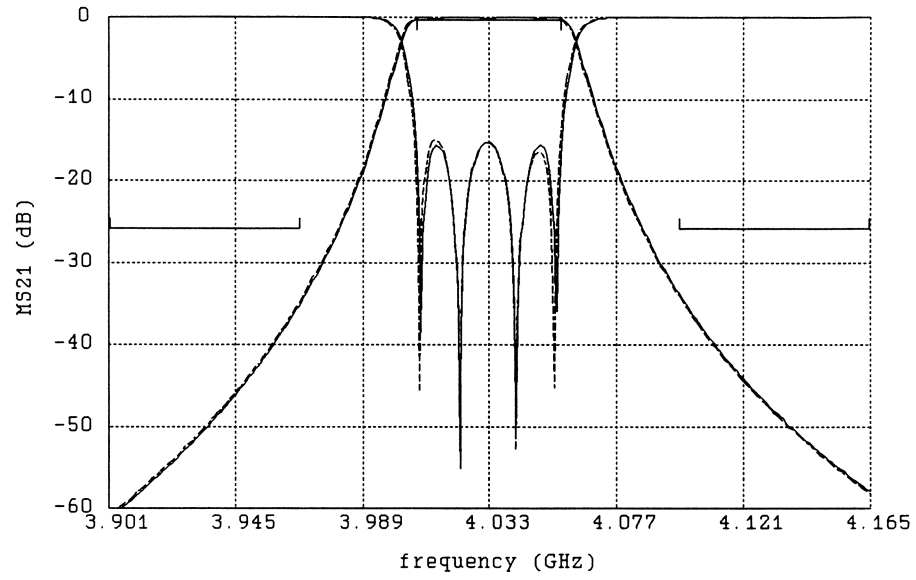

(a)

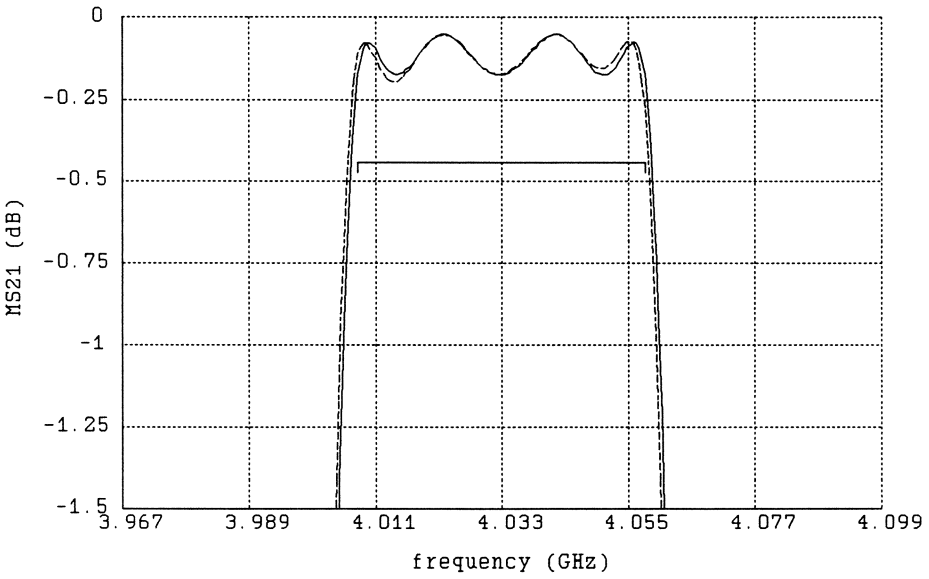

(b)

Fig. 8. (a) The $|S_{21}|$ and $|S_{11}|$ empirical model responses for the case (a) (——) and case (b) (---) minimax solutions. (b) The passband details of the $|S_{21}|$ responses.

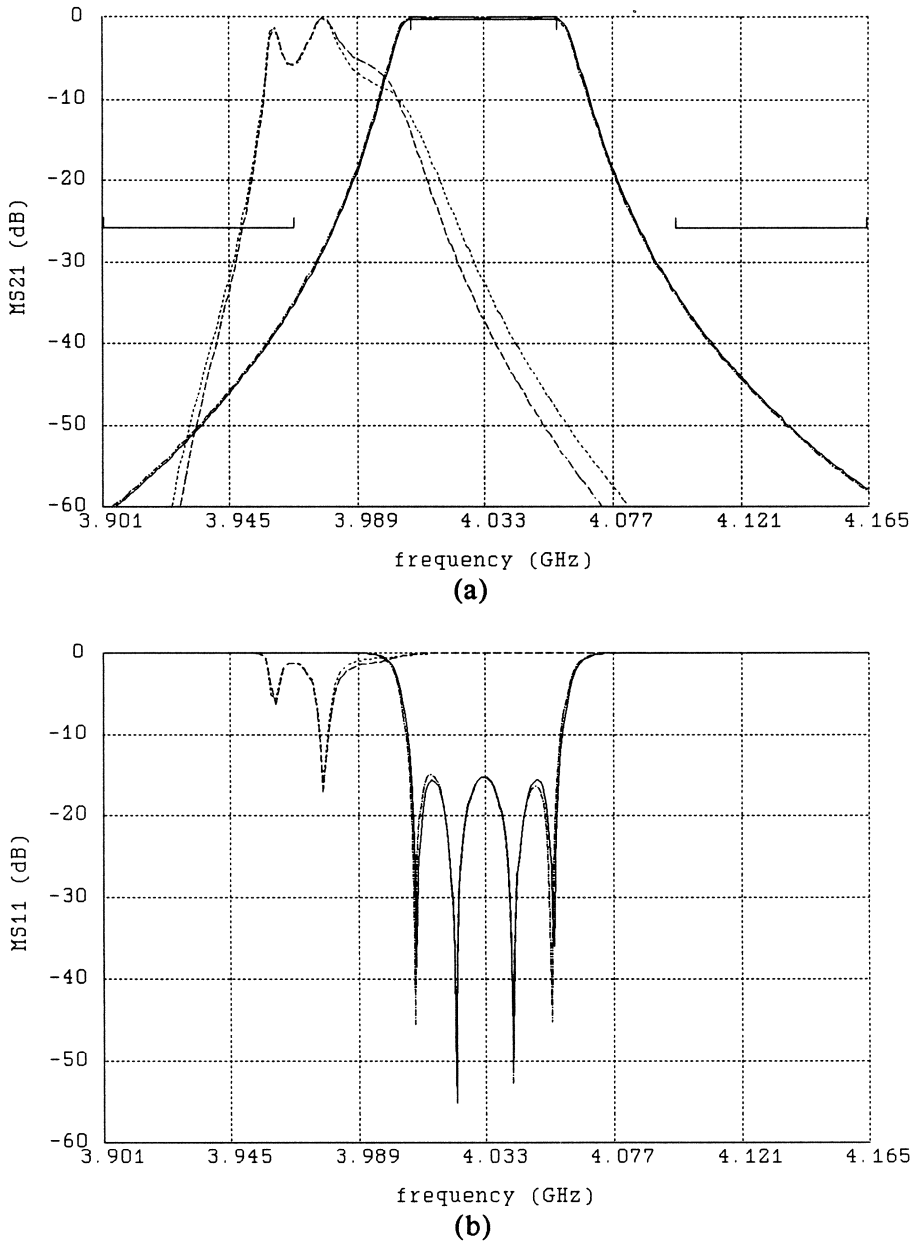

Fig. 9. A comparison between the (a) $|S_{21}|$ and (b) $|S_{11}|$ empirical model and corresponding ***em*** responses at the two minimax solutions.

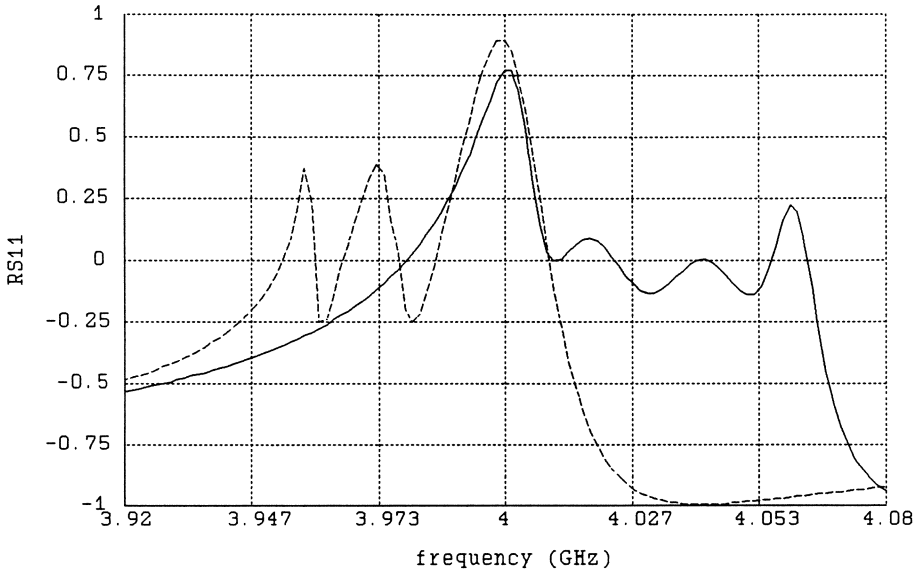

Fig. 10. Re$\{S_{11}\}$ simulated using the empirical model (——) and ***em*** (---) at the starting point before parameter extraction optimization.

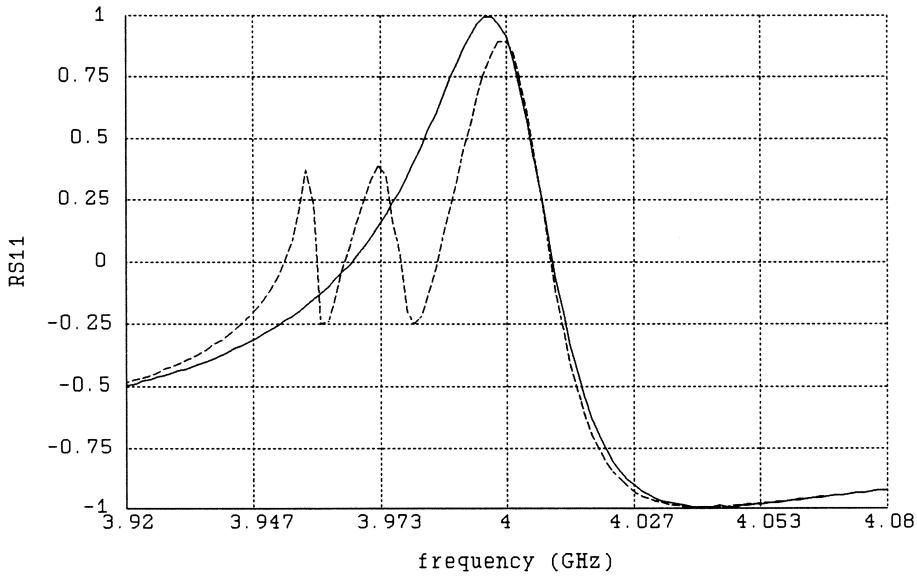

Fig. 11. Re$\{S_{11}\}$ simulated using the empirical model (——) and ***em*** (---) at the solution of a straightforward ℓ_1 parameter extraction optimization (a local minimum).

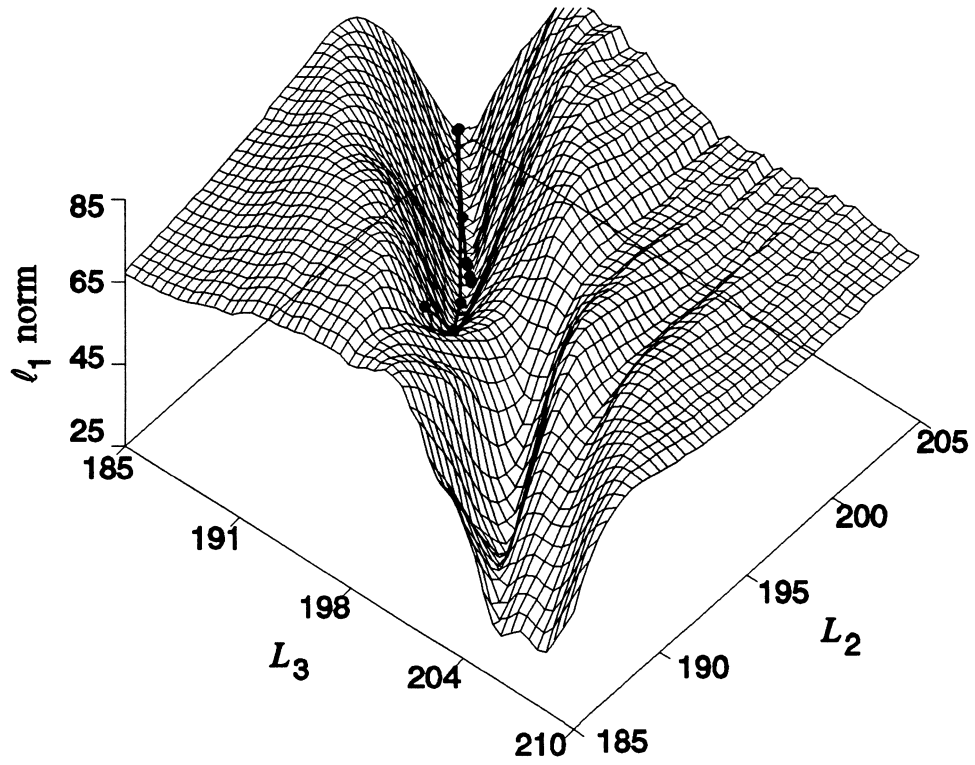

Fig. 12. Visualization of the ℓ_1 norm versus two of the model parameters L_2 and L_3, superimposed by the trace of the straightforward ℓ_1 optimization. The optimization converged to a local minimum instead of the true solution represented by the valley near the front of the graph.

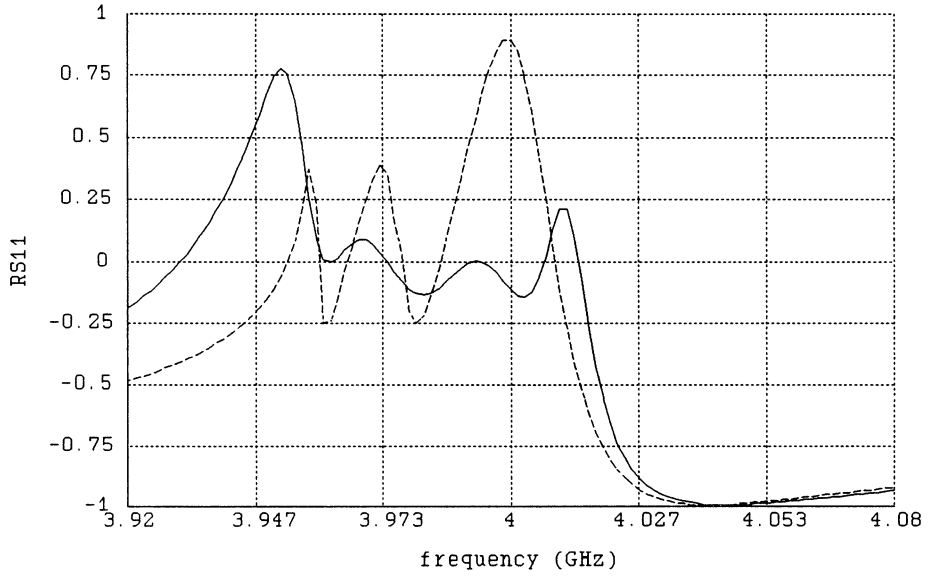

Fig. 13. Re$\{S_{11}\}$ simulated using the empirical model (——) and *em* (---) after *Phase* 1 of the FSM algorithm.

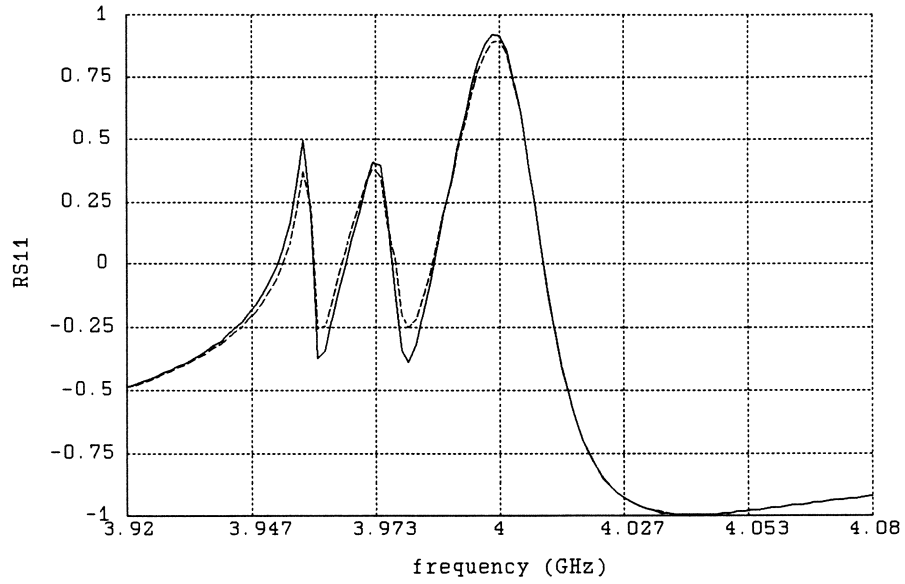

Fig. 14. Re$\{S_{11}\}$ simulated using the empirical model (——) and ***em*** (---) after *Phase* 2 of the FSM algorithm.

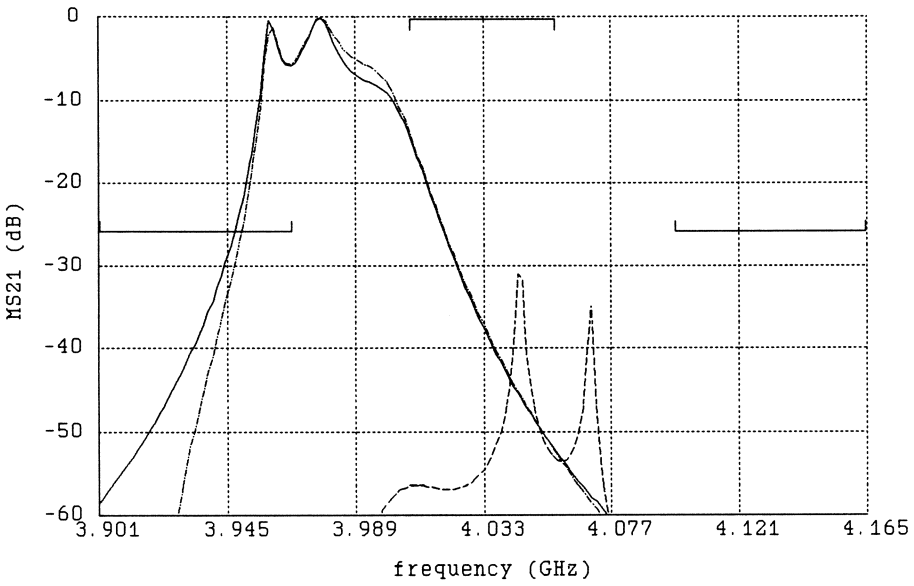

Fig. 15. The $|S_{21}|$ response match after a straightforward ℓ_1 optimization (---) and after using our new SFSM algorithm (——). The goal is the ***em*** model response, shown as (-·-). The straightforward ℓ_1 optimization has failed to generate a useful parameter extraction solution.

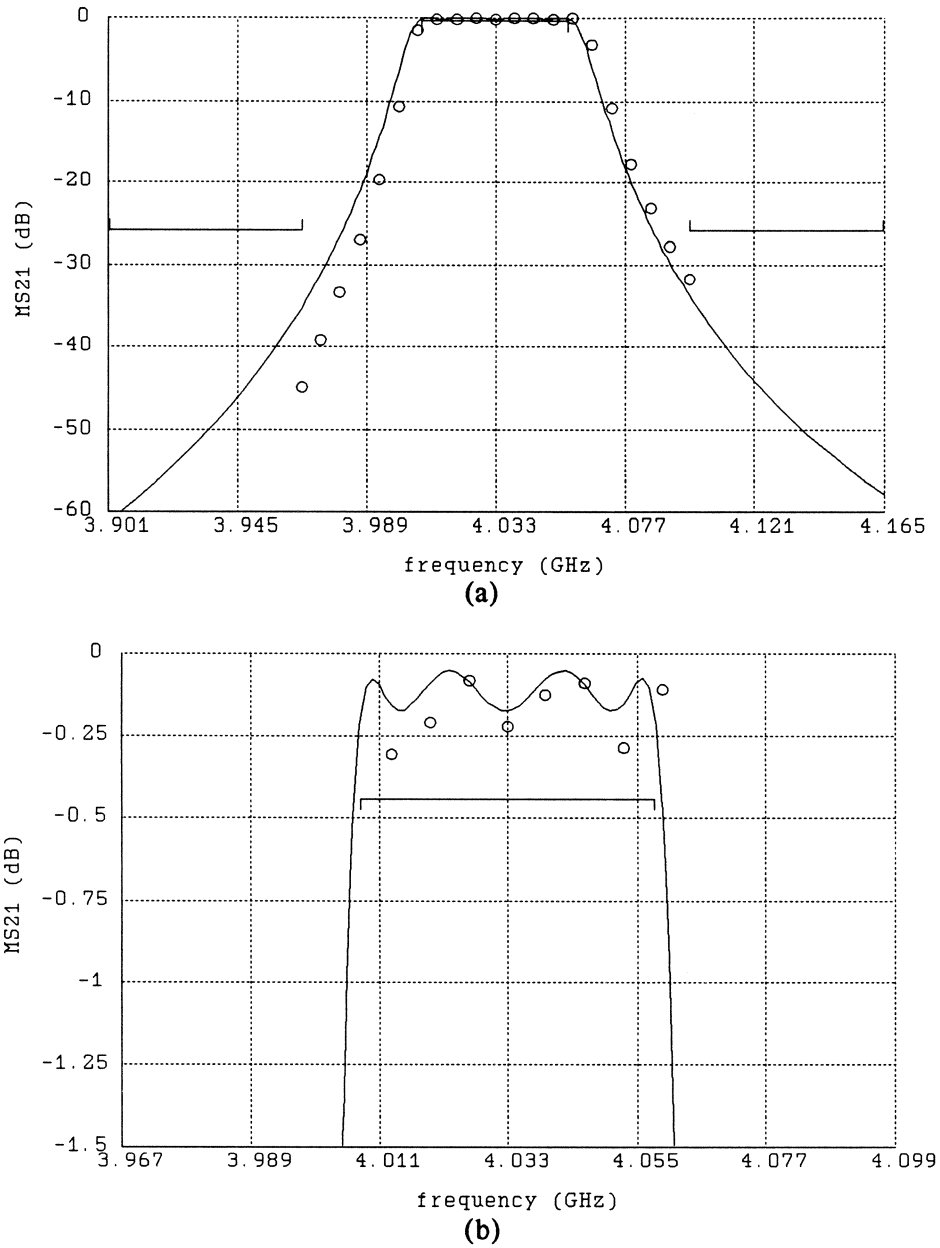

Fig. 16. The ***em*** simulated $|S_{21}|$ response of the HTS filter at the solution obtained using the quasi-Newton SM optimization method (○). The OSA90/hope empirical model solution (——) is shown for comparison. Responses for (a) the overall band and (b) the passband in more detail.